

# Hydrologic Characterization of Desert Soils with Varying Degrees of Pedogenesis: 1. Field Experiments Evaluating Plant-Relevant Soil Water Behavior

John R. Nimmo,\* Kim S. Perkins, Kevin M. Schmidt, David M. Miller, Jonathan D. Stock, and Kamini Singha

To assess the effect of pedogenesis on the soil moisture dynamics influencing the character and quality of ecological habitat, we conducted infiltration and redistribution experiments on three alluvial deposits in the Mojave National Preserve: (i) recently deposited active wash sediments, (ii) a soil of early Holocene age, and (iii) a highly developed soil of late Pleistocene age. At each, we ponded water in a 1-m-diameter infiltration ring for 2.3 h and monitored soil water content and matric pressure during and after infiltration, using probes and electrical resistivity imaging (ERI). Infiltration and downward flow rates were greater in younger material, favoring deep-rooted species. Deep-rooted species tend to colonize the margins of washes, where they are unaffected by sediment transport that inhibits colonization. The ERI results support important generalizations, for example that shallower than 0.5 m, infiltrated water persists longer in highly developed soil, favoring shallow-rooted species. Soil moisture data for the two youngest soils suggested that saturation overshoot, which may have significant but unexplored hydroecologic and pedogenic effects, occurred at the horizontally advancing wetting front. Spatial heterogeneity of soil properties generally increased with pedogenic development. Evidence suggested that some early-stage developmental processes may promote uniformity; the intermediate-age soil appeared to have the least heterogeneity in terms of textural variation with depth, and also the least anisotropy. Lateral heterogeneity was pronounced in older soil, having a multitude of effects on the distribution and retention of soil water, and may facilitate certain water-conserving strategies of plants over what would be possible in a laterally homogeneous soil.

ABBREVIATIONS: ERI, electrical resistivity imaging; TDR, time-domain reflectometry.

**D**ESERT PLANTS use different strategies to survive and flourish with erratically available water (Hamerlynck et al., 2002; Lombardini, 2006). The persistence of soil water within a particular depth range and its characteristic time scales of fluctuation (Katul et al., 2007) help determine the resulting plant community. The depth to which infiltration percolates and the degree to which water is retained at particular depths affect the relative advantage of shallow-rooted grasses compared with deep-rooted shrubs. The deeper unsaturated zone below the upper soil layers, including bedrock, can supply much of the water needed by many plants (Sternberg et al., 1996). Hamerlynck et al. (2002), investigating the contrasting water-use strategies of two codominant desert shrubs, found strong correlations between soil characteristics and the two species' densities and health. These

factors are of heightened importance in arid climates, where much time may elapse between significant infiltrations. Directly, as well as indirectly through its effect on plants, soil water affects the habitat of animals, which in turn influence the patterns of soil water behavior through activities such as burrowing.

Among the soil attributes affecting the ability of different parcels of soil to transmit, concentrate, distribute, and store water are heterogeneity and anisotropy. In dry regions, the lateral flow and distribution of water is important at small spatial scales (Grayson et al., 2006). Shafer et al. (2007) and others have observed substantial systematic differences in soil hydraulic characteristics between intercanopy and undercanopy areas. Grayson et al. (1997) noted a dominance of vertical over horizontal flow except under the wettest conditions; areal variation in soil properties is likely to substantially influence the distribution of water during periods of high soil moisture following rain or flood. Both heterogeneity and anisotropy, although frequently neglected or oversimplified in models of unsaturated-zone hydraulics, play an important role in structuring the ecosystem.

Soil developmental processes are critical to the characteristic hydraulic behavior that influences a soil's ability to support plant species and ecosystems. In desert soils, pedogenic development alters such attributes as clay and silt content, stoniness, soil structural type, degree of heterogeneity, and prevalence of macropores, which strongly influence the infiltration, redistribution, and retention of water. At the land surface, biotic crusts and desert pavement vary in consistent ways with the age of the deposit and are important influences on runoff, infiltration, and evaporation

J.R. Nimmo, K.S. Perkins, K.M. Schmidt, D.M. Miller, and J.D. Stock, U.S. Geological Survey, 345 Middlefield Rd., Menlo Park, CA 94025; K. Singha, Geosciences Dep., 503 Deike Bldg., Pennsylvania State Univ., University Park, PA 16802. The use of brand names does not constitute endorsement by the USGS. Received 5 Mar. 2008. \*Corresponding author (jrnimmo@usgs.gov).

Vadose Zone J. 8:480–495  
doi:10.2136/vzj2008.0052

© Soil Science Society of America

677 S. Segoe Rd. Madison, WI 53711 USA.

All rights reserved. No part of this periodical may be reproduced or transmitted in any form or by any means, electronic or mechanical, including photocopying, recording, or any information storage and retrieval system, without permission in writing from the publisher.

from the soil. One apparent major effect of pedogenesis in deserts is to reduce vertical infiltrability under wet conditions (Nimmo et al., 2008; Shafer et al., 2007; Young et al., 2004; Caldwell et al., 2006). Progressive eolian deposition of silts and clays under desert pavements may play a strong role in this reduction (Shafer et al., 2007). Young et al. (2004) also observed that the characteristics of older soils cause them to retain water for a longer time in the upper parts of the soil profile, perhaps reducing susceptibility to drought.

A major portion of investigations of unsaturated-zone water in deserts have emphasized the subsurface hydraulics most important to contaminant transport or aquifer recharge issues rather than the near-surface water distribution and retention characteristics that are most relevant to the needs of plants. Where plants have been the motivating application, it has mostly been for agricultural purposes. Increasingly it is being recognized that the soil hydraulic characterizations needed for a natural system of diverse species differ from those of traditional monocultural agriculture. The needs of ecological science require further investigation of soil water from this perspective.

In most quantitative modeling of soil moisture dynamics, the soil is characterized in terms of the hydraulic properties of traditional unsaturated-flow theory: the hydraulic conductivity  $K$  as a function of water content  $\theta$  or matric pressure  $\Psi$ , and the water retention, the characteristic relation between  $\theta$  and  $\Psi$ . These properties can give information needed for small-scale spatial distribution of soil moisture but are complex and time consuming to measure. Even with soil that is fully characterized in this way, however, these properties themselves do not indicate the plant-relevant status of soil moisture directly, but rather through particular solutions of Richards' equation applied with assumptions of hypothetical, historical, or statistical inputs and outputs of water to the soil.

This study's main purpose was to experimentally observe a range of moisture dynamics in different soils and interpret the results with respect to (i) the influence of geomorphic features and the degree of pedogenic development on soil water and (ii) the characteristic patterns of soil water distributions in time and space as related to the ecohydrologic needs of plants in natural desert environments. Evaluation of habitat quality on an areal basis is the basic longer term objective of the landscape and ecosystem program of which this research is a part. Although it is desirable to have results applicable to large regions, small scales have to be considered directly. Caylor and Shugart (2006, p. 276) noted that "small-scale patterns of vegetation structure are highly organized by internal processes,

which operate at local scales." Our research emphasized the scale of plant variation, typically ranging from a fraction of a meter to several meters, rather than the smaller scales typical of core samples or the larger scales of remote sensing.

Our field experiments, implemented essentially identically at different locations, used artificial hydraulic perturbations in the form of ponded infiltration and redistribution experiments to investigate the effects of different pedogenic development on wetting-front travel speeds, heterogeneity, anisotropy, and preferentiality. We acquired dynamic  $\theta$  and  $\Psi$  data to be used in estimating  $K(\theta)$  and soil water retention by inverse modeling. The companion study (Mirus et al., 2009) developed a way to estimate these properties for application to desert ecohydrology, optimized with the soil modeled as a two-layer system that obeys Richards' equation. This study was directed toward the generalization of trends that are useful in understanding soil developmental processes in relation to hydraulic properties, and the hydraulic behavior of desert soils relevant to habitat quality and ecosystem function.

## Field Site

We chose to investigate three diverse locations, with down-fan slopes between 1 and 2%, on a bajada in the Mojave National Preserve in the eastern Mojave Desert, California (Fig. 1). These locations represent different deposits, referred to as active wash, Holocene soil, and Pleistocene soil. We chose them to represent a wide range of pedogenic and ecologic conditions mappable within the Globe, Hayden, and Tough Nut fan units that lie along the west side of the Providence Mountains, as shown in Fig. 2 (Miller et al., 2009). The Globe and Hayden fan source areas are primarily granite and gneiss, while the Tough Nut fan source area is limestone and gneiss. The Pleistocene soil is therefore mineralogically different from the active wash and Holocene soil.

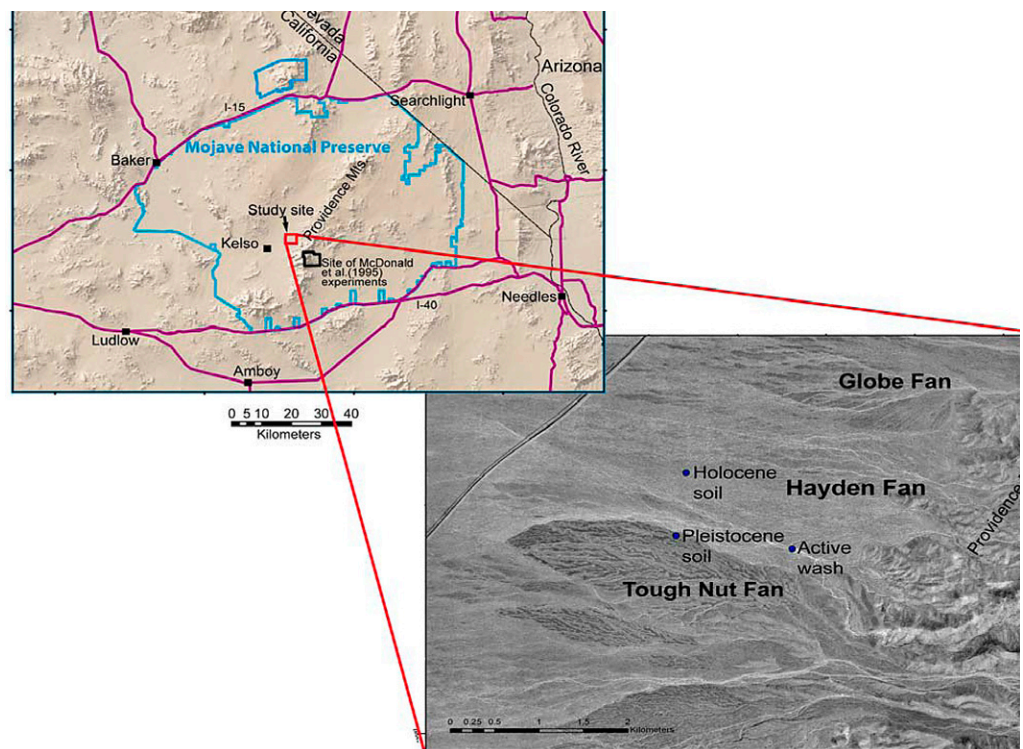


FIG. 1. Location of the study site including three experiment locations within the Mojave National Preserve, California.

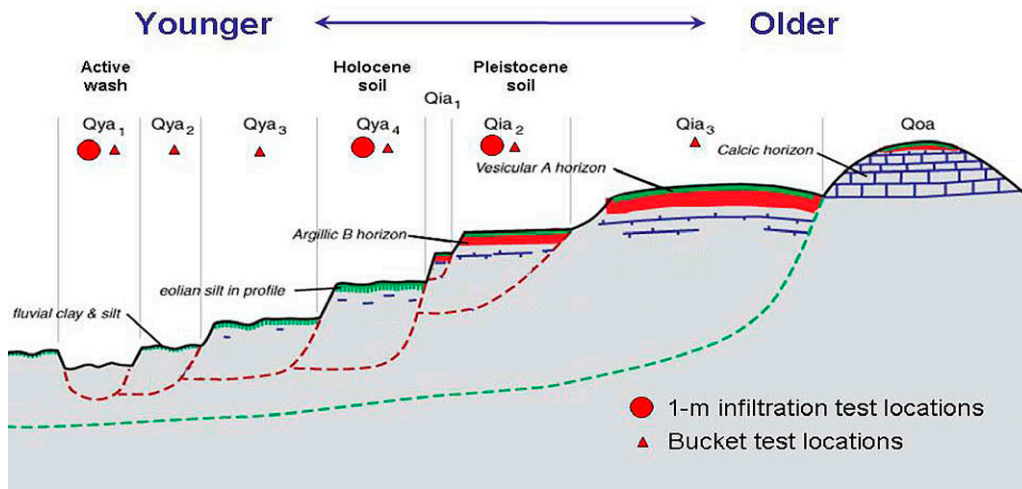


FIG. 2. Diagrammatic cross-section of alluvial terraces found in the Mojave National Preserve with symbols indicating the units of the three field test locations. The bucket test locations indicate units in which preliminary infiltrations were made during the process of site selection (Nimmo et al., 2008). For the terrace designations, Q indicates that the deposits are from the Quaternary period, y indicates a young deposit, i indicates an intermediate-aged deposit, and o indicates an old deposit. Numbers indicate increasing age within each of those three relative ages.

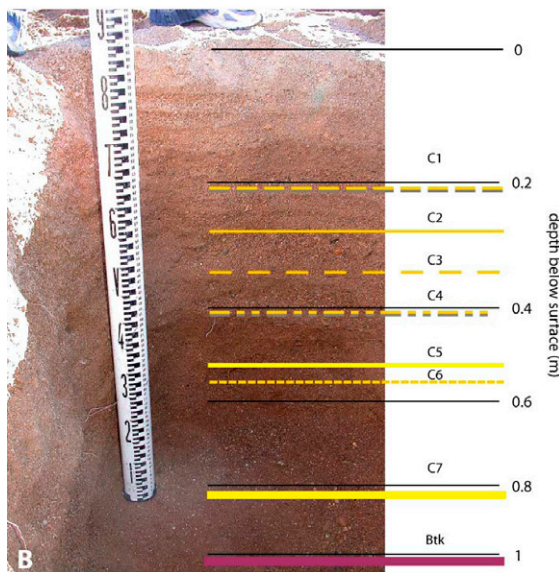


FIG. 3. Active wash: (A) view roughly northeast showing abundant creosote bush and horsebrush along the margins of the wash, 1-m diameter ring, instrumentation, water tank, and Providence Mountains in background; (B) hand-dug pit to depth of 0.84 m annotated with primary horizons. Colored lines denote base of horizon.

Distinctive surface characteristics and pedogenic properties of the selected deposits (Fig. 3–5) allow them to be mapped confidently, which provides a basis for extrapolating our findings throughout the broader area. Table 1 summarizes the characteristics of the deposits at the three field test locations. The active wash deposits are granular with significant open pore space, contain a paucity of clay and silt, and have well-stratified sandy beds from 1 to ~30 cm thick but no soil horzination. Layers due to different depositional events (C1–C7) are clearly visible (Fig. 3). The active wash is floored by an older soil horizon (Btk) at 0.84-m depth and fringed by creosote bush, *Larrea tridentata* (DC.) Coville, and shortspine horsebrush, *Tetradymia spinosa* Hook. and Arn.

The Holocene soil has weak to moderate desert pavement, a weakly developed silty and sandy Av horizon with little platy structure, and weakly developed Bw and Bk horizons that display considerable infilling by illuvial fines compared with the active wash. Shrubs of creosote bush and white bursage, *Ambrosia dumosa* (A. Gray) W.W. Payne, were present at the location of the Holocene soil. The late Pleistocene deposits have well-developed desert pavement and platy-structured Av horizons, moderately developed Bw and Bk horizons with noticeable silt and clay enrichment, and a cemented Btk horizon that exhibits Stage II to III calcic horizon morphology (Gile et al., 1966). White bursage shrubs were very sparsely present at the location of the Pleistocene experiment.

McDonald et al. (1996) demonstrated that increased limestone and dolomite in alluvial fan deposits result in more weakly developed Bt and Bw horizons and more strongly developed Bk horizons. These results are consistent with our observations of soils in the study area, where the active wash and Holocene soil located on the granitic fan have more reddened B horizons and weaker calcic horizon development than does the Pleistocene soil located on the fan rich in limestone. We interpret the relatively weak development of clay in the Pleistocene soil pit as owing to decreased incorporation of dust, in accord with McDonald et al. (1996).

## Experiments

### Preliminary Characterizations

Before the main infiltration and redistribution experiments, 28 smaller scale infiltration tests were conducted to aid in identifying suitable experiment locations as well as assessing spatial hydrologic variability (Nimmo et al., 2009). Soil samples were collected at numerous depths at the three designated test locations. Particle size distributions were measured for a total of 56 samples using laser diffraction for particles from 0.04  $\mu\text{m}$  to 2 mm and sieving for particles >2 mm. We collected five minimally

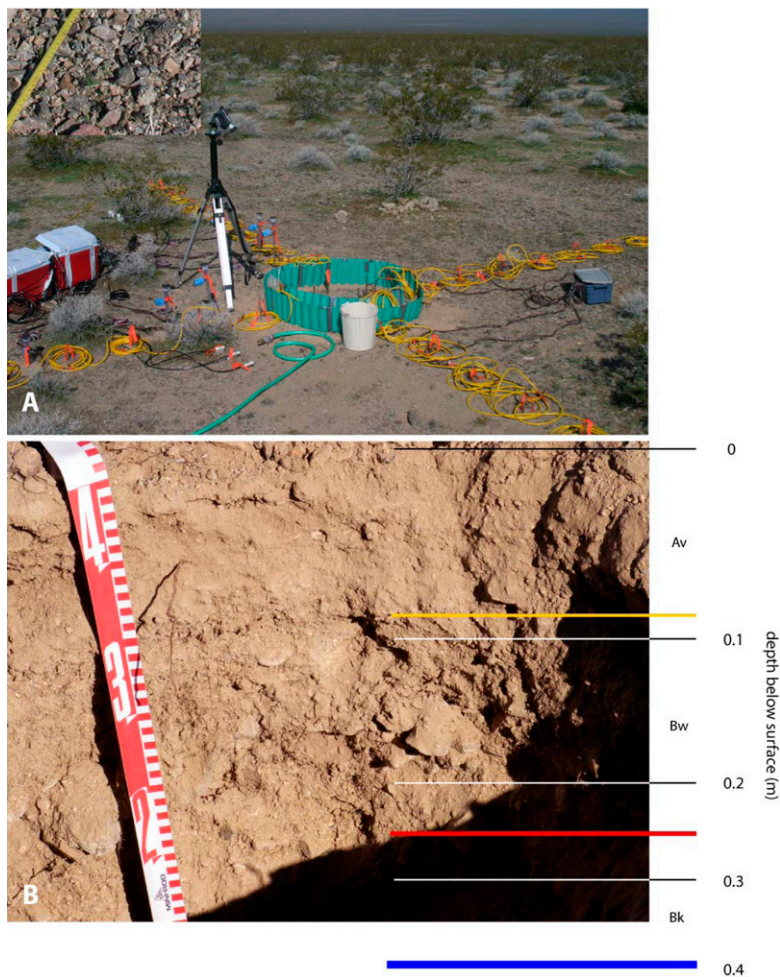


FIG. 4. Holocene soil: (A) view roughly west showing widely spaced shrubs of creosote bush and white bursage (smaller, grayish) on slightly hummocky surface with infiltration ring and instruments. Surface has weak to moderate pavement development with weak leveling of clast tops and weak packing (inset). Spaces between weak to moderately varnished clasts are filled with silt and sand or assemblages of lichens. (B) Annotated soil stratigraphy in hand-dug pit to depth of 0.4 m. Soil pits at different locations revealed moderate variability in the depth of the horizons, but the overall stratigraphic horizons were the same. Colored lines denote base of horizon.

disturbed core samples from the active wash and four from the Holocene soil. It was not possible to collect core samples from the Pleistocene soil because of its stoniness. The collected core samples' bulk density and particle density were measured, and also their water retention characteristics by the submersible pressure outflow cell method (Constantz and Herkelrath, 1984).

### Setup at Three Test Locations

To create a 1-m-diameter pond at each location, an infiltration ring was constructed of concrete between two concentric rings of corrugated plastic, 1.0 and 1.4 m in diameter. Nonmetallic materials were chosen so as not to affect soil electrical resistivity measurements. The soil between the rings was excavated to a few centimeters depth before pouring the concrete.

Subsurface probes for measuring  $\theta$  and  $\Psi$  were installed at various depths to 1 m in hand-augered boreholes at radial distances of 1.0, 1.5, and 2.5 m from the center of the pond in both cross-fan and down-fan directions (Fig. 6). We did not install any probes directly under the pond because doing so would

damage the hydraulically critical material at and below the floor of the pond. Attempts to use diagonal boreholes to position probes under the pond failed because of the noncohesive character of the sandy and stony materials. Water content was monitored using the soil dielectric constant measured by two types of instruments: two-electrode time-domain reflectometry (TDR) probes (Model 615, Campbell Scientific, Logan, UT) as well as wafer-type probes (Model EC-20, Decagon Devices, Pullman, WA). Matric pressure was monitored using tensiometers and heat-dissipation probes (HDPs). The TDR probes were driven into undisturbed material at the bottom of each hole. The EC-20 probes were placed at shallower depths within the holes as they were back-filled. The flexible-wafer design of these probes did not permit their insertion into undisturbed soil. Surrounded by disturbed material, the EC-20 probes would not be useful for indicating the absolute  $\theta$  of the soil but rather for relative changes in wetness with time. The water-content probes respond fast, giving a realistic picture of the time dependence of wetting and draining. The HDPs, however, which require moisture equilibration between the porous material of the device and the adjacent soil, respond in a matter of hours or days, and so are not useful for the early, fast-changing conditions. Matric pressure measurements from these probes were useful in inverse modeling to estimate unsaturated hydraulic properties (Mirus et al., 2009).

We used ERI to record subsurface resistivity with time. For measurement of resistivity, 48 electrodes were inserted to several centimeters depth in two intersecting lines, symmetric about the infiltration ring (Fig. 6c). One line was oriented by eye to align with the locally determined fan axis. The other was perpendicular to this line. The electrodes were spaced 0.5 m apart, the lines therefore extending to radii of 5.75 m from the pond center. Having all electrodes at the surface instead of in boreholes limited the depth sensitivity of the array to about 1.2 m. Borehole installation was not feasible because of possible damage to the wilderness area in which the experiments were performed. A number of data sets (15 in the active wash, three in the Pleistocene soil) were collected before infiltration to indicate the background resistivity. Data for each line were collected independently, alternating between the cross-fan and down-fan lines. Data were collected using a hybrid geometry ranging from skip 0 to skip 6 (i.e., with zero to six electrodes skipped between the electrodes used for the measurement) as described by Slater et al. (2000). To keep the speed of data acquisition reasonably high, for each tomogram the number of measurements was limited to 80 unique measurements on each line, and reciprocal measurements, with current and potential electrodes swapped, were not collected. A complete set of measurements required 8 min per line, so tomograms were made 17 min apart when the system was run continuously. To produce images of subsurface resistivity, the resistance data collected in the field were inverted with the commercially available code Res2DInv using the least-squares weighted misfit between observed and predicted measurements and a flatness-based measure of solution complexity (Daily and Owen, 1991; LaBrecque

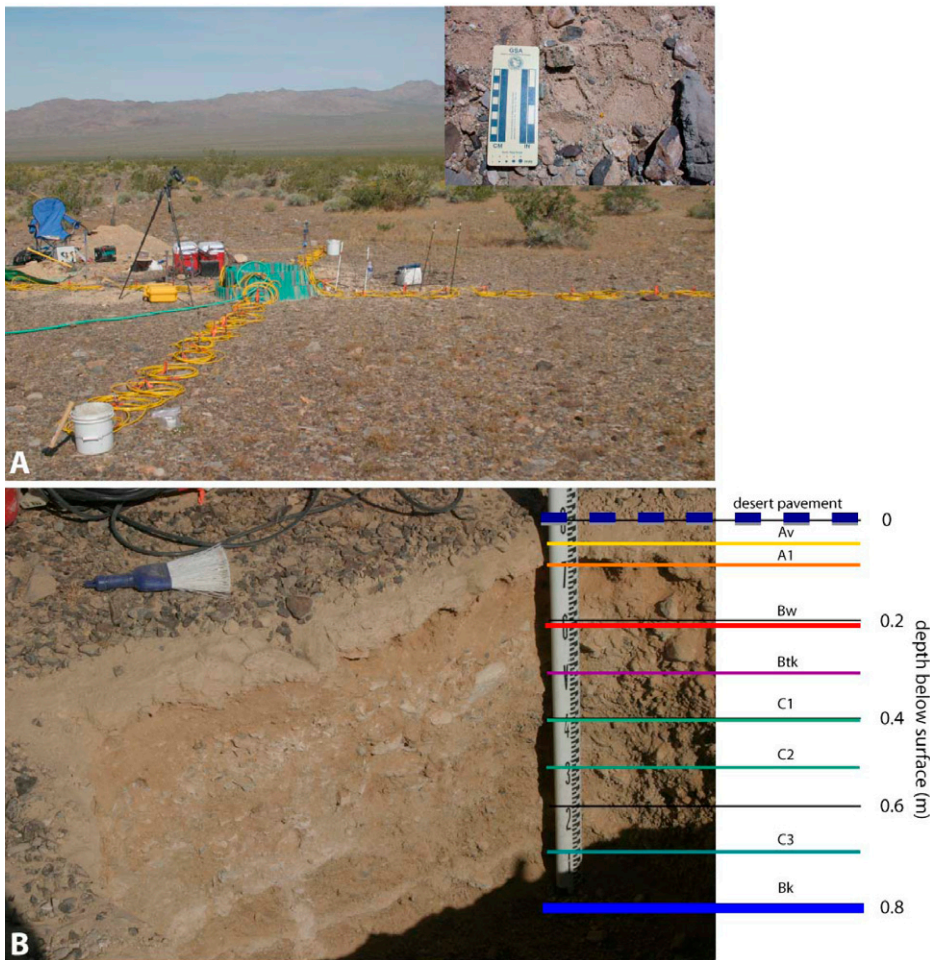


FIG. 5. Pleistocene soil: (A) view roughly west showing very sparse white bursage and instrument array in desert pavement with Kelso Mountains in background. Inset showing Av horizon under varnished clasts of desert pavement. (B) Hand-dug pit at instrument site used to define stratigraphic horizons. There was a general coarsening of soil texture to south end of pit toward bar top exposed on surface. Colored lines denote base of horizon.

et al., 1996; Tripp et al., 1984). The data for each time step were simultaneously inverted using the background data set as the reference model for inversion. The difference between the averaged inversion of the background data and the inversion from each time step was calculated to show the change in resistivity since artificial infiltration started. Assuming that during the experiment changes in  $\theta$  are dominant over changes in salinity or temperature, this change in resistivity indicates a change in  $\theta$ , inversely and nonlinearly. Although battery failure and program loss in the field prevented the use of ERI for the Holocene soil, images were successfully obtained for the active wash and Pleistocene soil.

Water for infiltration was from a well in Kelso (Fig. 1), the nearest site available, chosen as being less likely to alter measurements and properties than would water from a more purified or more external source. It was fed by gravity from a 1640-L cylindrical tank elevated about 1 m off the ground. A pressure transducer placed near the bottom of the tank indicated the level for computing the volume infiltrated with time.

### Procedure

At each test location, the inflow valve was opened at a designated zero time and additional water was immediately poured from buckets into the ring to bring the pond level up to 5 cm in <1

min. Flexible plastic temporarily placed on the soil surface minimized the soil disturbance related to pouring. The inflow valve was manually opened and closed to maintain the designated ponded depth. At each location, the constant-head phase of infiltration was terminated with final closing of the valve at 140 min. The remaining pond water infiltrated under falling-head conditions. Observations of the falling level with time and the disappearance of bulk water at the surface were recorded for continued estimation of the infiltration rate.

Soil moisture conditions were monitored from the onset of infiltration with all installed instruments. During infiltration, the ERI system was run continuously to collect information on the dynamically changing conditions. During redistribution, a complete measurement of the resistivity array was made every 2 to 3 h throughout the remainder of the initial day, and at least twice on each subsequent day for a total of 6 d. We monitored the subsurface moisture probes for 3, 2, and 4 mo at the wash, Holocene, and Pleistocene sites, respectively.

## Results

### Basic Characteristics of Three Test Locations

Textural data show that all three deposits have significant gravel (30–70%), with the percentage of silt and clay increasing with deposit age (Fig. 7). The very young deposits of the active wash exhibit intact depositional layering, while the Pleistocene soil has distinct layering as a result of complex soil-forming processes, including the effects of past climatic conditions, illuviation of silt, structural development, and accumulation of carbonate at depth. The Holocene soil has the least textural variation within the profile, possibly due to biogenic mixing of the original depositional layers and the slow rate of soil-forming processes.

At each test location, the infiltration rate was nearly constant, decreasing slightly with time in the active wash and Pleistocene soil (Fig. 8). Based on an average infiltration rate in each test (Nimmo et al., 2009), field-saturated hydraulic conductivity values  $K_{fs}$ , from youngest to oldest, were  $1.56 \times 10^{-4}$ ,  $8.91 \times 10^{-5}$ , and  $3.24 \times 10^{-5} \text{ m s}^{-1}$ . Infiltration capacity, the maximum rate at which water applied at the soil surface can infiltrate completely, is closely related to the  $K_{fs}$  for soil that has been thoroughly wetted but retains a certain amount of flow-path-obstructing air trapped within the soil pores. That  $K_{fs}$  was lower in the older soil, consistent with other studies cited by Nimmo et al. (2009), was expected because of higher fine-particle content and greater prominence of flow-impeding layer contrasts.

TABLE 1. Summary of soil properties for the active wash, the Holocene soil, and the Pleistocene soil.

Depth below surface m	Description of primary horizon
Active wash	
0–0.22	C1, thin-bedded medium fine sand
0.22–0.30	C2, poorly sorted medium sand with pea gravel
0.30–0.36	C3, poorly sorted cobble-rich medium sand
0.36–0.42	C4, poorly sorted silty-clay-rich cobble and sand
0.42–0.51	C5, poorly sorted cobble-rich medium sand
0.51–0.54	C6, well-sorted medium sand
0.54–0.84	C7, well-sorted coarse grussy sand; no apparent stratification.
0.84–1.04	Btkb, reddish oxidized silt and clay rich with oxidized slightly weathered clasts; moderate to high consistency with calcic stringers and clay films coating grains (represents erosional unconformity exposing older intermediate-age Quaternary horizon)
Holocene soil	
0	Incipient weak to moderately varnished pavement
0–0.09	Av, incipient sandy A horizon with few vesicles ~1 mm in diameter; weak platy structure in the upper 6 cm, a few layers with weak to enhanced clay films, skins, and bridges
0.09–0.25	Bw, weak faint reddening, weak consistence; clasts have powdery calcite on base but no hard calcite coats
0.25–0.40	Bk, Stage I or I– calcic horizon; hard calcite rims on base of most clasts with a few cemented together, providing weak cementation throughout horizon
Pleistocene soil	
0	Varnished gravel pavement with some cobbles, mix of carbonate and plutonic source material
0–0.06	Av, significant ped structure (~5–7-cm wavelength), strong vesicles ~2–4 mm in diameter, and silt-rich texture; blocky and platy structure.
0.06–0.10	A1, silty sand without vesicles, minor CaCO <sub>3</sub> stringers, some 2-mm-diameter roots extend to base of horizon with sharp boundary
0.10–0.22	Bw, moderate reddening, rotted disaggregated clasts and split clasts composed primarily of plutonic rocks, gravel, and cobbles
0.22–0.32	Btk, weak argillic texture but more cohesive than C horizon below, Stage I+ CaCO <sub>3</sub> coating (Holocene in age?), minor calcic stringers, gravel and cobbles, fine 1-mm-diameter roots extend to base of horizon; violent HCl reaction
0.32–0.40	C1, coarse sand and gravel, minor Stage I coating, no illuviation of fines
0.40–0.51	C2, gravel and coarse sand
0.51–0.71	C3, Stage I+ calcic coating with stalactites, minor cementation
0.71–0.8	Bk, Stage III+ calcic horizon with pore filling carbonate but no laminations; some calcic stringers, oriented both horizontally and vertically; violent HCl reaction

### Point Measurements with Subsurface Probes

Each instrumented borehole gave a time sequence of measurements for the probes at the various depths. Figure 9 shows the early (0–300-min) behavior of the water-content probes in all six of the closest (1-m radius) boreholes. The earliest TDR readings (although not the EC-20 measurements, in the absence of an absolute calibration) indicate antecedent conditions. The active wash experiment was affected by rain 2 d before, although very little water from that event remained in the upper portions of the deposit that were most important to the experiment. As there were no probes within the radius of the infiltration ring, the probes in these six holes serve as the best available proxy for soil water behavior under the pond. Owing to preferential flow, spatial variability of soil properties, and other factors, these data do not show a simple depthwise progression of wetting fronts. Several probes suggest the phenomenon of saturation overshoot, discussed further below.

Figure 10 shows the wetting front arrival time, the first significant increase of  $\theta$  above background, at each water-content probe. Arrivals were fastest in the active wash. Twenty-five of 34 probes at this location responded to infiltration, with all first arrivals occurring between 10 and 1320 min after the start of infiltration. For both the Holocene and Pleistocene soils, the first arrival came after 42 min. Initial responses to infiltrated water, however, occurred during an interval of only 510 min in the Holocene soil (with 19 of 30 probes responding) but an interval of  $8.6 \times 10^4$  min (60 d) in the Pleistocene soil (with 18 of 33

probes responding). For probes that detected the added water, the average travel times to a distance of 1 m from the pond center were 30 min for the active wash, 63 min for the Holocene soil, and 170 min for the Pleistocene soil. To a distance of 1.5 m from the pond center, average travel times were 120 min for the active wash, 370 min for the Holocene soil, and  $1.3 \times 10^4$  min (8.9 d) for the Pleistocene soil. Average travel times to a distance of 2.5 m from the pond center were 650 min for the active wash and  $4.8 \times 10^4$  min (33 d) for the Pleistocene soil. The wetting front was not detected beyond the 1.5-m distance at the Holocene site.

### Surface Electrical Resistivity Imaging

Figure 11 shows a representative selection of the differenced tomograms, giving a set of cross-sectional views of the changes in electrical resistivity associated with the changes in  $\theta$  through time. The average error in data measurements, based on stacking (repeatability), was generally <1%. Data on the cross-fan line were obtained about 8 min before data for the paired image on the down-fan line.

In the active wash, about 60 ERI data sets were collected along the two perpendicular lines. Both lines show a relative dominance of vertical with respect to lateral flow; little impediment to vertical flow appears in the uppermost meter. The maximum change in resistivity during the test was –135%. Because the soil was initially somewhat wet from antecedent rain, resistivity decreases as well as increases from the background data are

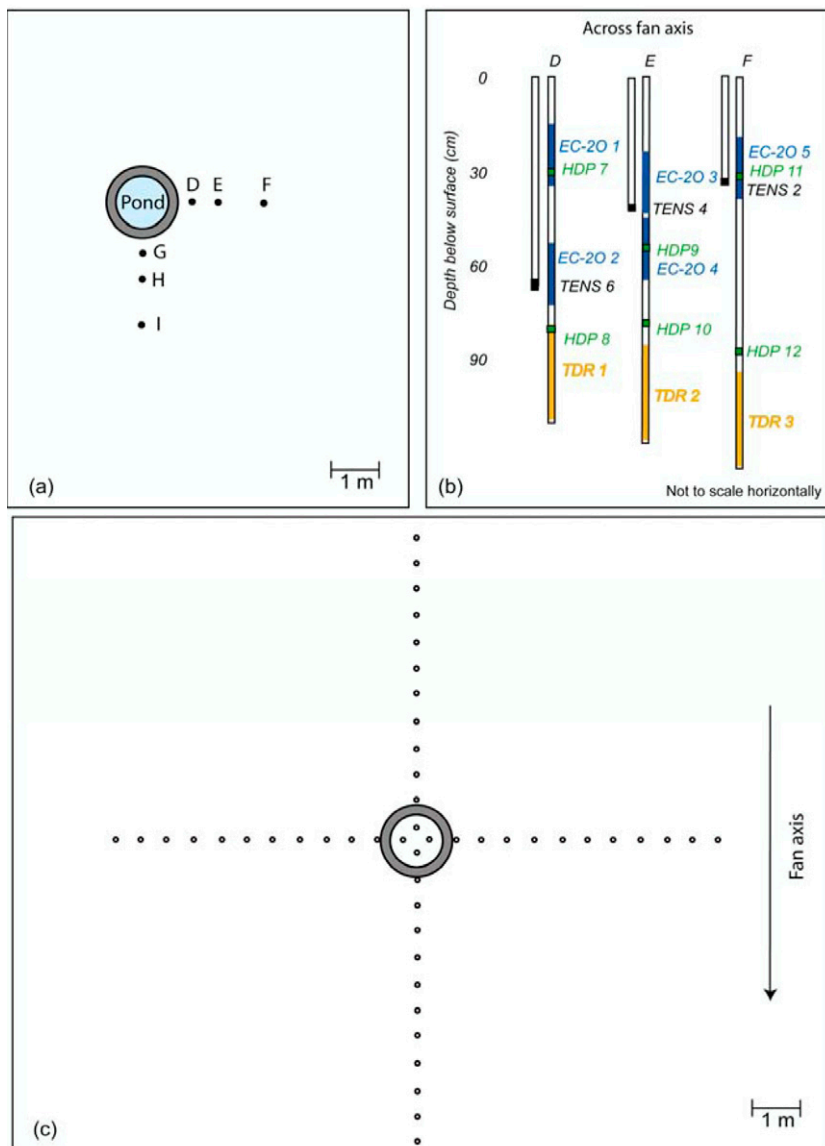


FIG. 6. (a) Map view of pond with locations of subsurface instrument holes. (b) Cross-section of typical probe installation depths (EC-20 and TDR are dielectric constant probes for water content, TENS are tensiometers, and HDP are heat dissipation probes for matric pressure); colored regions indicate the linear extent of the sensitive portion of each probe. (c) Map view of pond with locations of electrical resistivity imaging electrodes.

visible, and the final image indicates soil moisture drier than the antecedent conditions. Because an overparameterized model was used to construct the tomograms, we cannot exactly delineate the boundaries of the bulb of infiltrated water; however, it appears that during the 6 d of ERI operation, little water moved horizontally farther than about 1 m from the outer edge of the pond. The tomograms indicate that this bulb was relatively continuous, as expected given the relatively homogeneous structure of the active-wash deposits. The changes in electrical resistivity from the infiltrated water were mostly but not entirely gone from the ERI domain by 48 h after the start of the test.

In the Pleistocene soil, 36 ERI data sets were collected. Unlike the images from the active-wash experiment, which show a relatively smooth wetting front and quick movement of the fresh water through the soil, these show a more complex

distribution of water and slower flow. The ERI results are consistent with the smaller volume of water infiltrated into this soil. About one-fourth as much water infiltrated during this experiment, which at the end of infiltration appeared to be spread through about one-fourth as much wetted volume of soil. Water movement was mostly slower in this medium. An important exception, which gives evidence for preferential flow, is that in the first few minutes of infiltration, significant wetting occurred to about 0.4-m depth at two or three positions very near the pond (Fig. 11). Six days after infiltration, images show that resistivity remained significantly reduced in some portions of the ERI domain, indicating a persistence of the added water in some places at shallow depths. The maximum change in resistivity was  $-150\%$ , about the same as for the active wash. The tomograms show a more heterogeneous distribution of water in this soil, and it appears that the moisture stayed largely confined within shallow layers. The pattern of change through time is different; rather than a clear augmentation and dissipation of  $\theta$ , at some locations we see an apparent slow increase in  $\theta$  with time throughout the test. At the pixel scale, we find that fractional changes in resistivity approximately match changes in moisture mapped by co-located moisture probes, despite the difference in support volume and spatial and temporal resolution of the two types of measurement.

The total change in resistivity through time indicates how quickly moisture dissipates in the system. We do not attempt a spatial moment analysis here, as has been completed in other studies (e.g., Day-Lewis et al., 2007; Singha and Gorelick, 2005; Binley et al., 2002), because current flow travels out of the two-dimensional tomographic plane, making estimates of mass, center of mass, or spatial variance inaccurate. While we could proceed assuming axial symmetry of the two-dimensional profiles, the fact that the inverted images “see” resistivity reductions from parcels of soil moisture that are out of the plane will cause overestimation of the added water volume. Even without ERI-based quantitative estimates of the infiltrated volume, however, it is clear that the tomograms are sensitive to the increase and subsequent dissipation of infiltrated water.

## Discussion

### Hydraulic Behavior of the Different Soils

As expected,  $K_{fs}$  declined with increasing soil development. The difference, however, is a modest factor of 5 for the youngest and oldest soils, even though the youngest lacks observable development of soil horizons. This result is consistent with small soil-age-related differences in  $K_{fs}$  observed by Caldwell et al. (2006). The  $K_{fs}$  in the active wash may be smaller than expected for a homogeneous medium, possibly because of a hydraulic retarding effect of layered structure that results from episodic

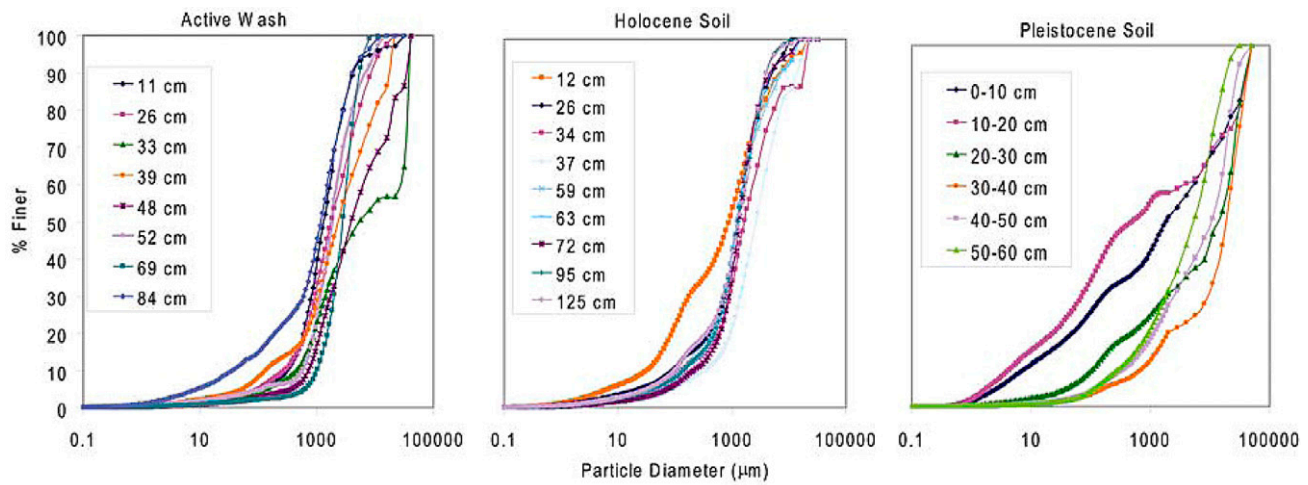


FIG. 7. Particle-size distributions at various depths from the three field test locations.

deposition (Fig. 3b). As indicated by visual observation and by evidence of more uniform texture with depth (Fig. 7), the Holocene soil may have a relatively homogeneous vertical structure, suggesting that some of the early pedogenic processes tend to reduce rather than enhance layer contrasts, for example the vertical mixing resulting from long-term burrowing by ants, reptiles, and rodents. Another factor reducing age-related contrasts is that the Pleistocene soil, although highly stratified and having a pronounced  $A_v$  horizon, probably has a large number of small macropores (e.g., related to platy or blocky soil structure) that facilitate downward flow.

In the active wash and Holocene soil, wetting fronts were generally sharper than in the Pleistocene soil, and increases in  $\theta$  persisted significantly only where there were older, buried soil horizons. In the Pleistocene soil, the elevated  $\theta$  persisted through the 4-mo monitoring period (Fig. 12), suggesting (i) that in soils affected by both macropores and strong layer contrasts, the flow-retarding influence of the layers may dominate in the long term,

and (ii) that the very sparse vegetation at this site did not extract all available water during this period.

Layer contrasts are expected also to enhance lateral flow. This effect has some support from the ERI results in Fig. 11: the wetted portion of the soil is somewhat wider in the more stratified Pleistocene soil than in the active wash, especially after a day of redistribution. For the Holocene soil, although there are no ERI results to compare, there is further evidence for less lateral flow and therefore less influence of stratification, in that none of the six water-content probes at 2.5 m from the center indicated a wetting front arrival, whereas five showed wetting at this position in the active wash and three in the Pleistocene soil (Fig. 10).

Other investigators have found similar trends. In a layered and macroporous silt loam soil, Nimmo and Perkins (2008) observed that the influence of macropores diminished to negligibility at 2.5-m depth, whereas the hydraulic effect of layer contrasts continued at greater depths, suggesting a comparable long-term hydraulic dominance of layer-contrast impedance over downward macropore flow. Hamerlynck et al. (2002) found a younger soil to allow greater downward flow and an older soil to have more lateral flow with less drainage from the upper horizons. Lohse and Dietrich (2005) observed these same trends in soils of a humid region.

Figure 11 shows much more heterogeneity in the Pleistocene soil than the active wash. This comparative result was expected, given that the very recent deposits of the wash were laid down in layers by processes that, within the active area, were not very sensitive to variation with position. Certain parcels within the Pleistocene soil, mostly with a volume of a fraction of  $1 \text{ m}^3$ , became markedly wetter or drier than their immediate surroundings. The asymmetry of their positions suggests that they resulted from the preexisting nature of the subsurface material as opposed to the water-inflow geometry of our experimental setup.

Both diffuse and preferential flow are in evidence. The generally orderly wetting processes observed in the probe, infiltration, and

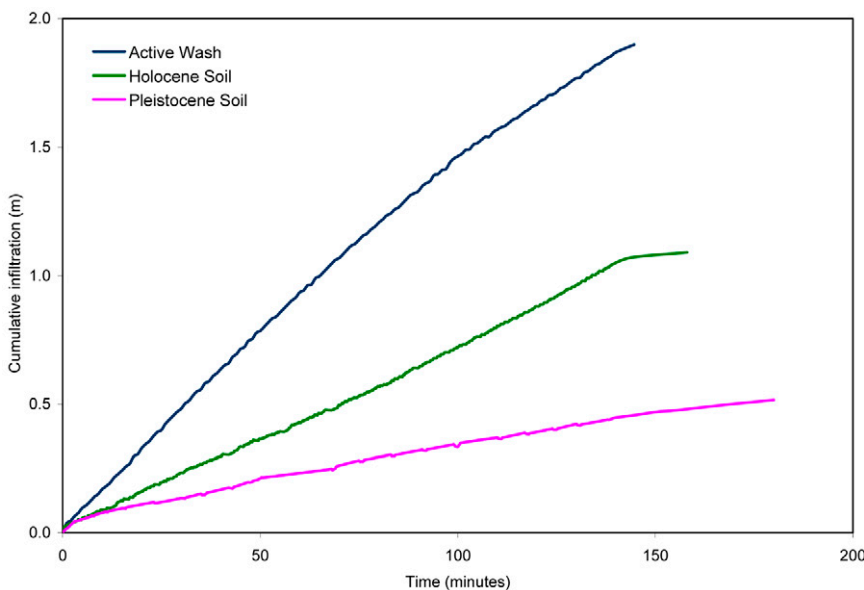


FIG. 8. Cumulative infiltration with time for the three field test locations.

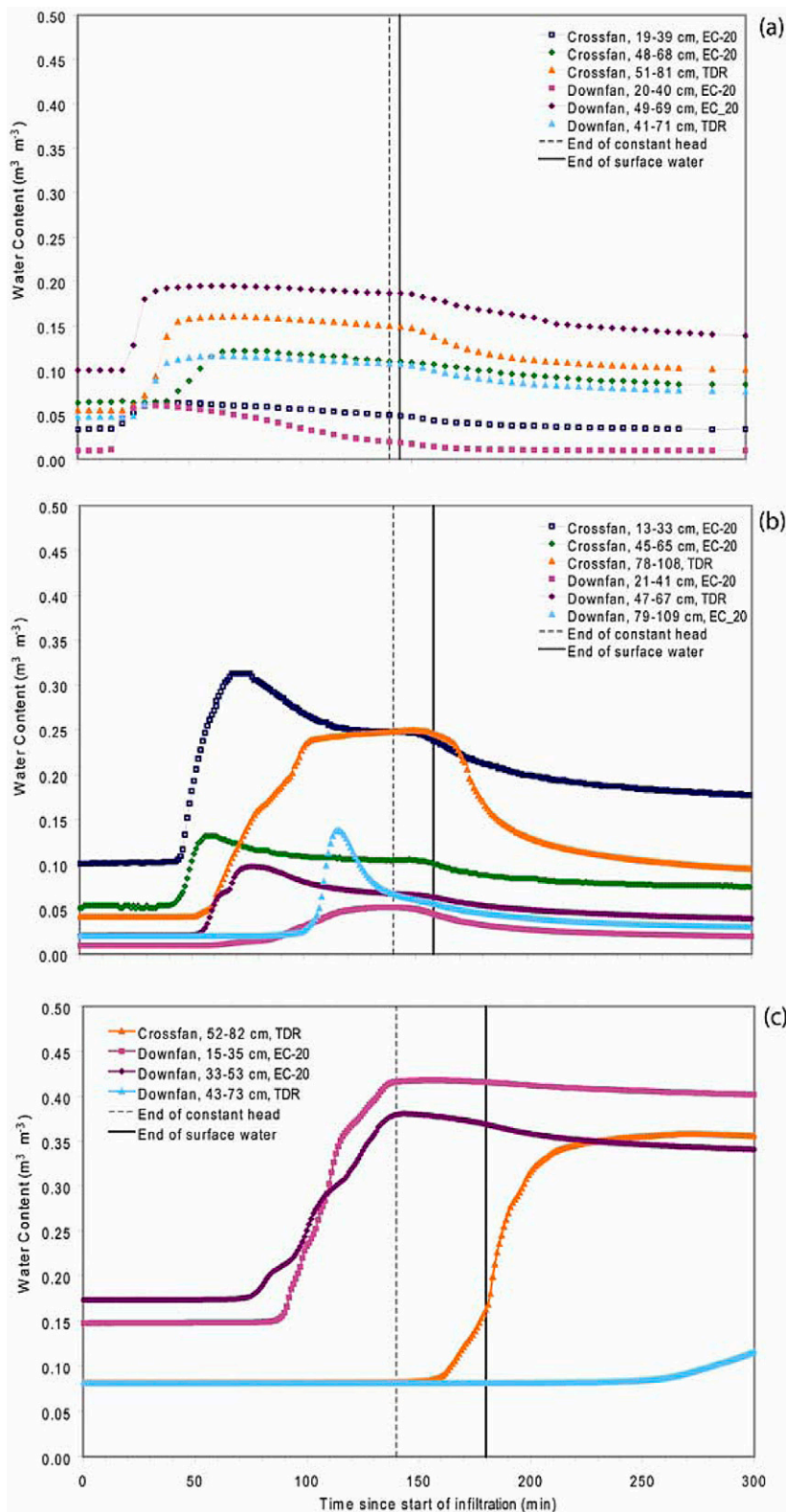


FIG. 9. Changes in water content with time for the instruments located 1 m from the pond center in (a) the active wash, (b) the Holocene soil, and (c) the Pleistocene soil. The dashed vertical line indicates the end of constant-head ponding and the solid line indicates the time at which all surface water had infiltrated (EC-20 and TDR are dielectric constant probes).

ERI results suggest diffuse flow. The variation in arrival times, shapes, and amplitudes in data from close-in probes (Fig. 9) suggests that flow is preferential or at least strongly affected by

small-scale heterogeneity. As in the dye tracer results of Meadows et al. (2008), evidence for preferential flow is stronger in the older soil. In the Pleistocene soil during the early portions of the infiltration period (Fig. 11), for example, rapid wetting of some parcels of soil in the 0.2- to 0.4-m depth range occurred before observable wetting of the soil above and around these parcels. The preferential flow paths conveying water from the pond to these wetted parcels are probably too narrow to be detectable in the ERI results. Given the point-like nature and relatively sparse spacing of the probes, and the limited ERI resolution, preferential flow may have been more prevalent in these experiments than the measured data indicate.

### Evidence and Implications of Saturation Overshoot

In the  $\theta$  values indicated by all the probes located at a radius of 1.0 m (Fig. 9), saturation overshoot is apparent from the several cases where  $\theta$  peaked before the end of constant-head infiltration (2.3 h). This phenomenon occurs if, after rising in response to a steady input of water,  $\theta$  at a subsurface point declines significantly before the water input rate diminishes. This behavior occurs despite the prediction of standard Darcy–Buckingham–Richards unsaturated zone flow theory that  $\theta$  will increase monotonically as long as the infiltration rate does not diminish. Our measurements provide evidence of saturation overshoot in the two younger deposits and are inconclusive for the Pleistocene soil. Table 2 summarizes data related to saturation overshoot at each of the water-content probes at 1-m radius. The magnitude of overshoot may be inferred from the difference in  $\theta$  between its peak within the period of constant-head infiltration and its value at the end of that period. In Table 2 such a measure, called the *overshoot relative amplitude* (ORA), is computed as the fraction of overall net change in  $\theta$  represented by the peak-to-final difference in  $\theta$ :

$$ORA = \frac{\theta_p - \theta_f}{\theta_f - \theta_i} \quad [1]$$

where  $\theta_p$ ,  $\theta_i$ , and  $\theta_f$  are the peak, initial, and final (end of constant-head infiltration) values of  $\theta$ . Values of ORA exceeded 0 for the six probes of the active wash and four of the six probes of the Holocene soil.

Other causes may contribute to the peaking of the wetting front documented in Fig. 9 and Table 2. A pulse of salinity carried by the wetting front could influence the soil moisture probes in a way that would cause their  $\theta$  readings to increase (Baumhardt et al., 2000). Reduced salinity behind the front could then cause a decline in the readings. Little salinity was apparent at these shallow depths, however, especially in the active wash and Holocene soil materials, so this is unlikely to have caused the entire degree of overshoot that

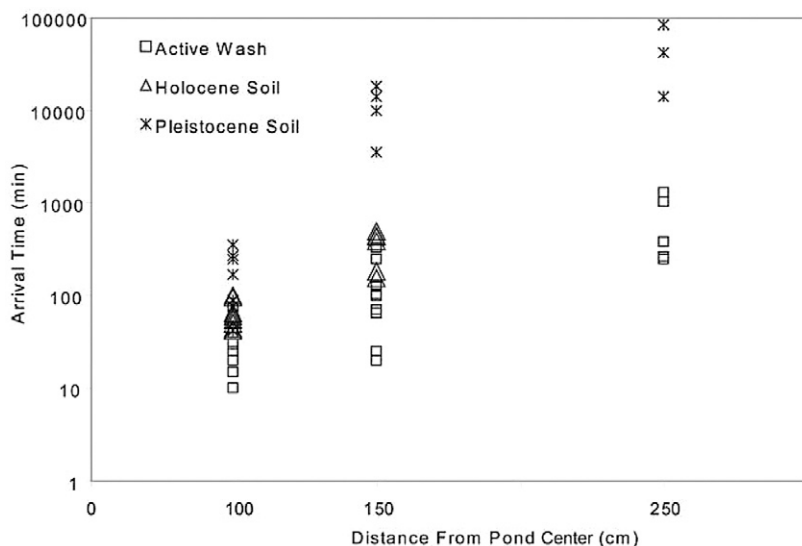


FIG. 10. Arrival time of wetting front observed with water content probes at distances of 1, 1.5, and 2.5 m from the pond center at the three field test locations. Water did not reach the 2.5-m probes at the Holocene site.

appears in Fig. 9. There is also the possibility that preferential flow may have caused early  $\theta$  peaks, but it seems unlikely for a single preferential flow path to register the observed  $\theta$  change in a probe whose response represents an average along the 20-cm probe length, and to do so for a large proportion of the probes. Similarly, temporary localized perching at layer boundaries may cause such peaking, but this would be improbable for so many of the probes, especially since much of the flow to the probes was parallel to the primarily horizontal stratification.

The occurrence of saturation overshoot is well documented in laboratory experiments and in relatively homogeneous media (DiCarlo, 2006; 2004; Shiozawa and Fujimaki, 2004; Stonestrom and Akstin, 1994). Our measurements suggest that it occurs also in natural settings and heterogeneous media. Under ponded infiltration it may in fact be common, considering that it is apparent in two of the three soils and from 10 of the 15 water-content probes that could have detected it. It might have been observed also at the other five probes if the infiltration had been sustained longer than 2.3 h. Saturation overshoot can occur in fingered wetting front behavior, but the evidence in this experiment suggests nonfingered or large-fingered flow in that saturation overshoot was seen at a substantial majority of the probes closest to the pond, and that these probes are physically large with respect to the typical widths of fingered-flow channels.

Practical consequences of saturation overshoot have been little studied. It is conceivable that the pulse of higher than normal maximum water content may serve an ecologic function, for example if a brief pulse of extra-wet conditions plays a role in seed germination or other aspects of plant physiology. Shiozawa and Fujimaki (2004) showed that a wetting front with saturation overshoot can temporarily cause essentially total saturation of the soil, a condition that in desert soil might otherwise never occur. It could play a pedogenic role, for example if the decline in matric pressure after passage of an overshooting wetting front in an Av horizon caused dissolved air to effervesce and create vesicles (e.g., Hillel, 1998, p. 406). Evidence for saturation overshoot in lateral flow, as suggested by the configuration of our pond and probes,

is of interest because it would show that gravity is not essential to create the condition of piled-up water just behind the wetting front. There may be considerable value in investigating the prevalence of saturation overshoot in natural situations, and its possible hydrologic, ecologic, and pedogenic effects.

### Ecohydrologic Use of Electrical Resistivity Imaging Data

The ERI results, even without a calibration in terms of absolute  $\theta$ , provide a strong indicator of soil morphology relevant to hydraulic dynamics that can support ecohydrologically significant generalizations. The spatially exhaustive character of ERI is especially important for evaluating heterogeneity at the submeter scale and for investigating a field plot in which it is not known in advance which parcels of soil will be of the most interest.

Electrical resistivity imaging inversions cannot quantify actual values of volumetric  $\theta$  because tomographic reconstructions are not point measurements but rather weighted local averages due to regularization criteria used within the inversion, survey geometry, measurement physics, and measurement error (Singha et al., 2007; Day-Lewis et al., 2005). The inherent spatial variability of the natural media, as well as the issues listed here, means that an independent calibration relation would be needed for every point in the domain, and the unknown calibration at each point may interactively affect others. Consequently, the conversion of field-scale tomograms directly to  $\theta$ , or any another hydrologic state variable, is usually incorrect; mass balance is often poor and estimates of tracer spread are too high. For example, in an ERI study to monitor a fluid tracer in the vadose zone, Binley et al. (2002) applied locally derived petrophysical relations to convert resistivity tomograms to changes in moisture content; their analysis revealed a 50% mass balance error that was attributed to the poor sensitivity in the center of the image volume where the tracer was applied. To avoid complications with correcting petrophysical relations to account for geophysical insensitivity (e.g., Moysey et al., 2005), we use the images in a more qualitative framework. As a surrogate for  $\theta$ , we use the negative of relative change in resistivity:

$$w(\rho) = - \left[ \frac{\rho - \rho_0}{\rho_0} \right] \quad [2]$$

where  $\rho$  is the resistivity and  $\rho_0$  is the background value of resistivity. The sign convention here means that  $w$  increases as  $\theta$  increases. Knowledge of the distribution of resistivity permits examination of the movement of a wetting front in multiple dimensions, the amount of time infiltrated water is retained at various depths in the subsurface, and the anisotropy of flow.

The ability of soil to retain a significant portion of added water long enough for effective use by plants is essential to determining the favorability of the soil for particular ecosystem components. Although seldom if ever applied to desert ecology, certain traditional agricultural characterizations may provide a useful starting point. Field capacity, the water content when downward percolation is considered negligible 2 or 3 d after

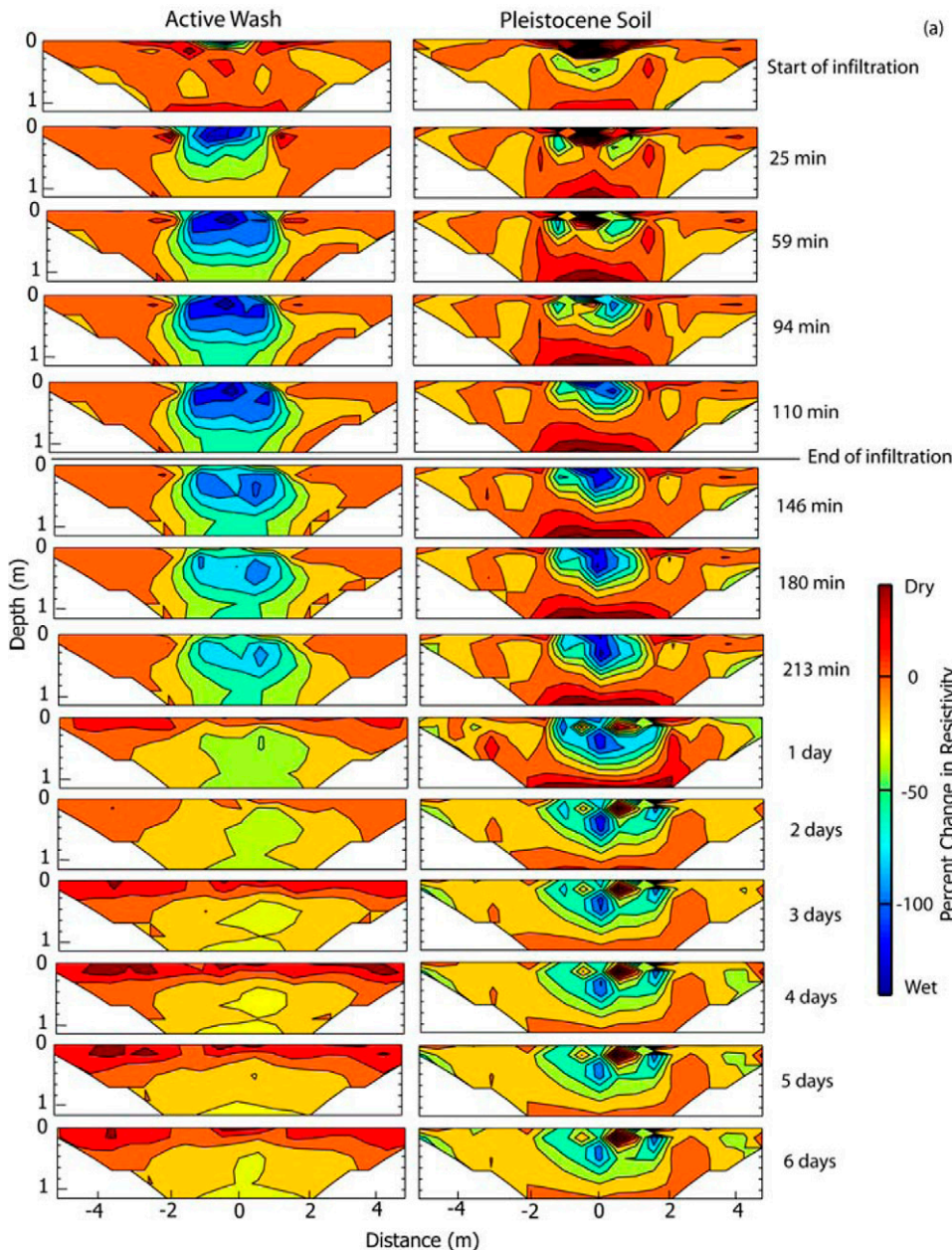


FIG. 11. Images of change in electrical resistivity at selected times during infiltration and redistribution at the active wash and Pleistocene sites, in vertical planes along the (a) cross-fan (oriented left to right looking upslope) and (b) down-fan (along the fan axis, left to right looking from upslope to downslope) directions. Vertical exaggeration is a factor of 1.8. Blank spaces correspond to times for which data were excessively noisy so that images could not be reliably computed. Figure continued.

substantial infiltration (SSSA, 1997), is used in estimating the upper limit of the amount of water available to plants. Water in excess of this value is assumed to drain away before plants have time to use it. Of the many definitions of field capacity in use, we chose that of SSSA because it is widely applied and accepted and it indicates plant-available water fairly directly rather than indirectly as through a designated value of matric pressure. The mention of “2 or 3 d” suggests a guideline for what typically might be considered negligible percolation in agricultural practice. Where greater precision is required, it may be taken as exactly 48 h (Cassel and Nielsen, 1986). A soil’s wilting point, the minimum  $\theta$  required to maintain a nonwilting plant condition, depends largely on a species-specific value of matric pressure. For many agricultural

species this value is commonly taken to be  $-1.5$  MPa, although among desert species it is more variable and in some cases often much drier (Odening et al., 1974). Schulze et al. (2005, p. 285), for example, gave a value of  $-3$  MPa for drought-adapted plants, while Andraski (1997) and Scanlon et al. (2003) measured matric pressures down to  $-8$  MPa in a root zone supporting growth of creosote bush. Available water, defined as the difference between field capacity and the wilting point, indicates roughly the amount of water from one event of major infiltration that the soil can supply for use by plants:

$$\theta(t) = \theta_p \exp(-t/\tau_\theta) \quad [3]$$

Figure 13 illustrates the decline of relative resistivity for a particular grid cell of the Pleistocene soil. The field capacity of soil at this position would be the water content that corresponds to the value of relative resistivity at 48 h. If the curve follows the pattern of exponential decay, meaning that the rate of loss slows in proportion to the amount remaining to be lost (Hillel, 1998, p. 451–452), then an alternative indicator is the time constant of the curve, i.e., the parameter  $\tau_\theta$ , where  $t$  is time and  $\theta_p$  is defined as in Eq. [1] and is analogous to the parameter  $\tau_w$  in

$$w(t) = w_p \exp(-t/\tau_w) \quad [4]$$

In general,  $\tau_w$  will not equal  $\tau_\theta$  but will have a one-to-one functional relationship with it, so a greater  $\tau_w$  indicates a greater  $\tau_\theta$  also. As a quantification of water-holding ability,  $\tau_\theta$  or  $\tau_w$  is easy to standardize and to calculate from time-series data. It is not known how repeatable such estimated time constants are, or whether an exponential model is the most suitable for this purpose. A further advantage of  $\tau_\theta$  or  $\tau_w$  is that even in cases such as ERI results where an absolute calibration of  $\theta$  is not available, it has a physical interpretation with dimensions of time. Determined from in situ measurements, the time constant is affected by root water uptake as well as the ongoing processes of drainage and redistribution. Like field capacity, an index of this nature cannot be defined for an isolated elementary volume of soil because for any volume of soil it depends on soil water behavior outside that volume (e.g., effects of flow-impeding layers that may be some distance away) as well as inside. It can be ecologically useful, however, because living organisms interact with the intact soil profile, not isolated volumes of soil.

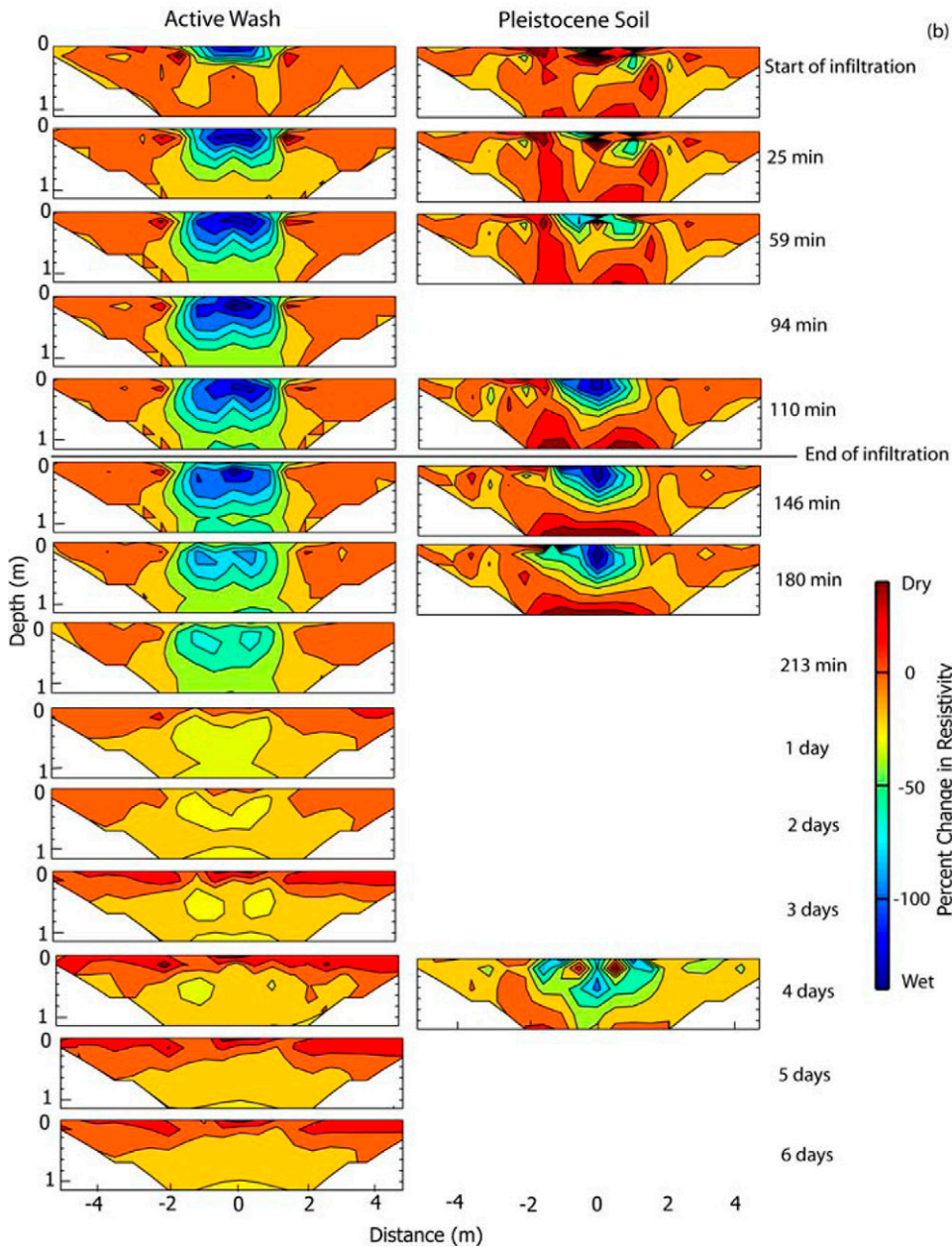


FIG. 11. Continued.

Using Eq. [4], we estimated  $\tau_w$  from the graph of  $w(t)$  for each ERI grid cell under or close to the pond. The  $w_p$  values were taken directly at the end of constant-head infiltration or at the peak of  $w$ , whichever was later in time;  $\rho_o$  values were taken as the average for the last few measurements in the data set, for which changes became negligible. Table 3 gives the time constants computed for grid cells out to 1.25 m, and Fig. 14 graphs the time constants for a portion of the domain that got substantially wetted.

The asymmetry that demonstrates that the heterogeneity is inherent to the subsurface material is strongly apparent from the time constants in Fig. 14. In particular, in the cross-fan direction, there is a parcel of soil, perhaps about 0.5 m in diameter, at about 0.2-m depth and 0.5-m radius on the right side of the infiltration pond, that wet particularly fast and thoroughly during infiltration and lost water quickly after infiltration (Fig. 11a, top five images). The time constant computed for this position is

(b) markedly lower than its left-side counterpart in Fig. 14. Assuming that the ring, which penetrated only about 5 cm into the soil, had minimal influence, the hydraulic properties of this volume of soil caused copiously supplied water to be easily transported into its large pores but held only weakly by capillary attraction against the force of gravity. The smaller time constant of this parcel suggests that its water-holding properties are more similar to the active-wash deposits than are those of the soil parcel to its immediate left. Farther to the right, at a radius of about 1.5 m, there is a similar-sized parcel of soil with contrasting behavior (Fig. 11a, Table 3); it tended to hold water by capillary attraction much more strongly than soil elsewhere in the domain. Such variations in the soil's ability to retain water may play a vital role in mediating the response of different plant functional types to the temporal distribution of precipitation that is a component of ecosystem-response models such as that of Ogle and Reynolds (2004).

#### Ecohydrologic Implications of Soil Water Heterogeneity

Some of the soil moisture processes deriving from lateral heterogeneity may have essential ecosystem functions. Breshears and Barnes (1999, p. 467), proposing a model that considers variations between laterally juxtaposed compartments of soil in addition to the more usual consideration of vertically juxtaposed layers, noted that "even small horizontal differences in volumetric water content may be important biologically" in part because a high sensitivity of  $\Psi$  to  $\theta$  creates a large  $\Psi$  variation under these circumstances. Ursino (2007, p. 8) has shown that lateral dispersal of soil moisture is important to the distribution of vegetation in areas subject to organization such as banding, and in particular that greater lateral flow "would eventually disperse the scarce resource and thus would not favor the vegetation organization." Variations have often been studied in terms of canopy and intercanopy areas (e.g., Bhark and Small, 2003). A common finding is that the infiltration capacity is greater at shrub locations than where the soil is bare. It remains unclear in many respects how geologic and biologic influences work together and in response to each other during soil development, raising questions concerning the extent to which soil properties develop and then dictate where plants will be, as opposed to plants themselves causing or enhancing soil lateral heterogeneity. In any case, lateral heterogeneity of soil

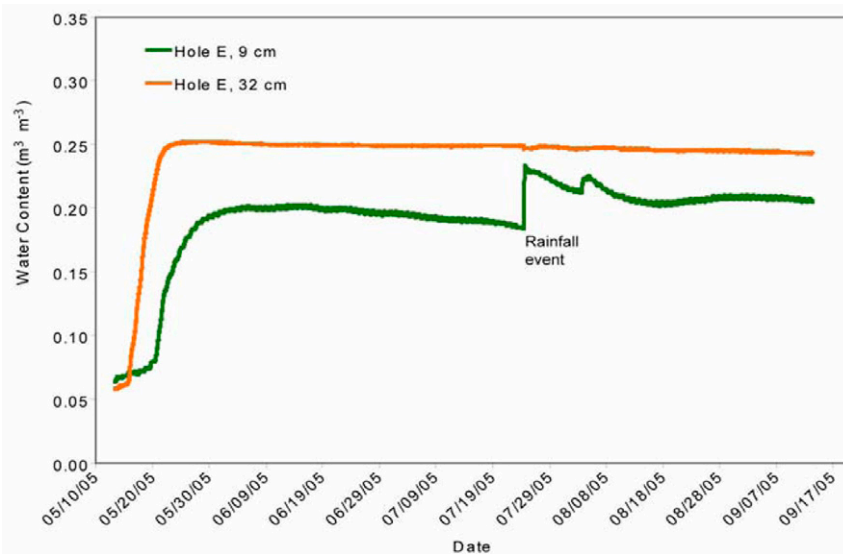


FIG. 12. Persistence of increased water content in the Pleistocene soil through the 4-mo monitoring period following the artificial infiltration experiment. The decline was very slow at both 9- and 32-cm depths, although the shallower soil was somewhat faster. The shallower soil was clearly more strongly affected by rainstorms in July 2005. The water content rise in response to the artificial infiltration, however, was faster in the deeper soil, suggesting perhaps that one or more preferential flow paths connected the surface to soil at the greater but not the shallower depth.

hydraulic properties is probably of great importance regardless of its relation to canopied or bare-soil areas.

The lateral heterogeneity of a transect as shown in Fig. 11a can be considered in terms of parcels in two broad categories: (i) soil that conducts water easily when wet, but maintains a high  $\theta$  only briefly, and (ii) soil that conducts water poorly when wet, but after wetting can maintain a high  $\theta$  for an extended time. As shorthand labels for discussion, these can be called (i) “transmissive” and (ii) “retentive” parcels of soil. Concerning the Av

horizon, if there are significant lateral variations in this horizon, these variations are part of the effect under discussion; if instead the Av horizon is relatively uniform, then soil below about 10 cm dominates the retentive–transmissive distinction. Transmissive soil has the characteristics traditionally associated with a sandy texture, while retentive soil has characteristics associated with silty and clayey textures. In actuality, various factors other than texture might cause the transmissive–retentive difference, for example macroporosity or hydrophobicity.

During rainfall, the transmissive soil, having greater infiltration capacity, should allow infiltration at a rate equal to or greater than the rate into the retentive soil. During high-intensity rainfall, localized runoff above retentive soil may infiltrate into an adjacent parcel of transmissive soil. Thus water content may increase much faster in the transmissive soil. That greater lateral heterogeneity causes overall greater infiltration capacity is known from measurements with different sizes of infiltration rings (Youngs, 1987).

For a time during and after rainfall, a given parcel of retentive soil would have a lower matric pressure than adjacent highly wetted transmissive soil and therefore would suck water out of the transmissive parcel (e.g., the parcels at 1.5- and 0.5-m lateral positions in the Pleistocene soil in Fig. 11a). During this process, the transmissive soil, being wet, has a relatively high  $K$ . There also would be downward flow, especially out of transmissive parcels of soil, although in practice further downward flow may be limited by an impeding layer at some depth. Impeding layers can effectively prevent preferential flow at depth, even in soil that is macroporous and fine textured (Nimmo and Perkins, 2008).

During the time interval up to the next infiltration, the retentive soil would retain most of the additional water that it absorbed out of the transmissive soil until it was used up, as by evapotranspiration. During this phase, direct evaporation from the transmissive soil would be minimized by its dry condition. Also during this phase, lateral movement from the wet retentive to dry transmissive soil is inhibited by the capillary barrier and low dry-soil  $K$  of the transmissive soil. Grayson et al. (1997) noted also that the lateral flow that occurs at higher water contents may become insignificant as the soil becomes drier. Thus the retentive soil has the possibility of taking in much of the water that infiltrates in adjacent parcels, and holding it with minimal loss to drainage and to lateral flow. This

TABLE 2. Early volumetric water content ( $\theta$ ) behavior at boreholes nearest the infiltration ring.

Orientation, depth, and probe	Depth (center of probe) cm	Time to peak $\theta$ min	Initial $\theta$	Peak $\theta$	$\theta$ at end of constant head	Overshoot relative amplitude
Active wash						
Cross-fan, 19–39 cm, EC-20	29	35	0.035	0.063	0.050	0.867
Cross-fan, 48–68 cm, EC-20	58	70	0.064	0.122	0.110	0.261
Cross-fan, 51–81 cm, TDR	66	60	0.055	0.160	0.150	0.105
Down-fan, 20–40 cm, EC-20	30	30	0.010	0.062	0.019	4.778
Down-fan, 46–66 cm, EC-20	56	60	0.100	0.195	0.187	0.092
Down-fan, 44–74 cm, TDR	59	55	0.047	0.116	0.107	0.150
Holocene soil						
Cross-fan, 13–22 cm, EC-20	23	68	0.102	0.312	0.248	0.438
Cross-fan, 45–65 cm, EC-20	55	56	0.054	0.132	0.105	0.529
Cross-fan, 78–98 cm, TDR	93	145	0.042	0.248	0.248	0.000
Down-fan, 21–41 cm, EC-20	31	130	0.010	0.052	0.052	0.000
Down-fan, 47–67 cm, EC-20	57	76	0.021	0.098	0.067	0.674
Down-fan, 80–110 cm, TDR	95	115	0.020	0.138	0.067	1.511
Pleistocene soil						
Cross-fan, 15–35 cm, EC-20	25					no data
Cross-fan, 41–61 cm, EC-20	51					no early data
Cross-fan, 52–82 cm, TDR	67	274	0.082	0.358	0.082	none
Down-fan, 15–35 cm, EC-20	25	146	0.148	0.417	0.417	0.000
Down-fan, 33–53 cm, EC-20	43	143	0.173	0.381	0.380	0.005
Down-fan 43–73 cm, TDR	58	1600	0.081	0.3	0.081	none

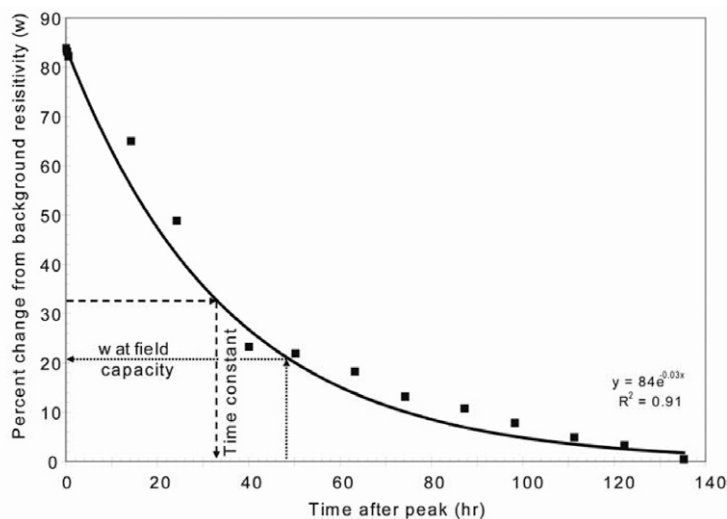


FIG. 13. Illustration of decline of relative resistivity (a proxy for water content) with time, showing how a fitted exponential curve relates to field capacity and to a time constant of exponential decline ( $\tau$ ). The relative resistivity here is for the grid cell of the Pleistocene soil cross-fan right side that was centered 0.75 m from the pond center at 0.44-m depth.

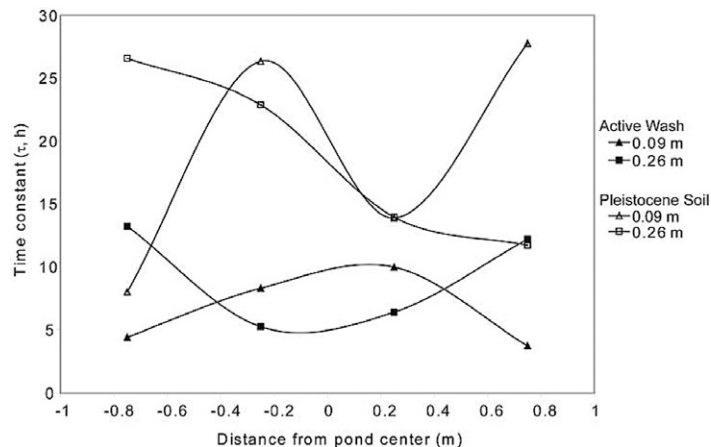


FIG. 14. Spatial variation of time constant  $\tau_w$  determined from electrical resistivity imaging (ERI) results for two depths of the cross-fan ERI plane in the active wash and Pleistocene soil.

TABLE 3. The time constant of moisture decline, estimated using electrical resistivity imaging, at various depths and positions near the infiltration ring, from -1.25 to 1.25 m from the pond center, in the cross-fan direction.

Depth m	Time constant of moisture decline					
	-1.25 m	-0.75	-0.25	0.25	0.75	1.25
	min					
	Active wash					
0.09	3	4	8	10	4	5
0.26	21	13	5	6	12	11
0.44	14	12	8	8	14	11
0.63	10	7	6	10	10	8
0.85	11	5	6	9	8	6
1.09	17	9	10	13	11	10
	Pleistocene soil					
0.09	increasing	8	26	14	28	765
0.26	flat	27	23	14	12	31
0.44	flat	28	342	300	33	106
0.63	flat	464	6	207	15	300
0.85	increasing	increasing	increasing	328	9	365

effect also would tend to reduce bare-soil evaporation, by causing most soil water to be stored under a fraction of the total area.

In the Pleistocene soil, ERI images in the down-fan direction (Fig. 11b) suggest a lesser degree of heterogeneity than the cross-fan images (Fig. 11a). Although from only one site, this evidence may stem from a systematic tendency toward more intense heterogeneity in the cross-fan direction, traversing the original sedimentologic depositional structure. The observed cross-fan vs. down-fan difference suggests that alluvial fan architecture may influence water availability in ways that are vital for plant and ecosystem health.

Soil moisture patterns affect root distributions and thus plant productivity, drought tolerance, and phenology. Concerning vertical heterogeneity, Hamerlynck et al. (2002) illustrated this with two plants that are present in our study area. White bursage, common in the Holocene and Pleistocene soils, draws water mainly from the 0- to 0.5-m depth that contains most of the infiltrated water in the Holocene and Pleistocene soils (Fig. 11). Creosote bush, common at the Holocene soil and along the margins of the active wash, on the other hand, can opportunistically root to greater depths, allowing uptake of water at depths >1 m. Thus it might be able to use much of the water infiltrated in the active wash, whereas white bursage would not. The water-retaining ability of fine-textured and stratified media would commonly reinforce these tendencies.

## Conclusions

Water flow in soils of different ages shows several prominent trends with soil development. Infiltration capacity declines with increasing age. The magnitude of decline is modest, however, consistent with features of pedogenic development (aggregation, horizonation, macropore creation, etc.) having complex and in some respects opposing influences. Having been made with a 1-m-diameter infiltration pond, the constant-head  $K_{fs}$  measurements were less affected by edge effects and are more inclusive of small-scale spatial variability than previously reported measurements done with bucket-sized infiltrometers (Nimmo et al., 2009). Depths reached easily by infiltrated water are reduced in older soils by the development of more pronounced stratification, despite the probable creation of additional preferential flow paths with time. The heterogeneity of soil hydraulic properties generally increases with pedogenic development, although with evidence that some of the early-stage developmental processes promote uniformity. The Holocene soil, for example, has in some ways the least heterogeneity, such as minimal textural variation with depth and also less apparent anisotropy. Electrical resistivity imaging tomograms show distinctly greater lateral heterogeneity in the Pleistocene soil than in the active wash, and to some extent an increased lateral spreading of infiltrated water indicative of greater profile-scale anisotropy.

Pedogenically altered hydraulic properties affect the soil's ability to sustain and nourish particular species. The active wash deposit has relatively little, and relatively homogeneous, ability to retain water with time. The Pleistocene soil overall has developed in ways that may somewhat reduce

the amount of water that infiltrates but that promote its accumulation and retention in fractional-cubic-meter-sized parcels of soil. This inhomogeneously retained water is likely to cause shallow-rooted plants to distribute themselves in response, possibly to near the edges of the more water-retentive parcels. A major open question is the degree and ways in which plants either create favorable soil characteristics or take advantage of those that already exist. The juxtaposition of retentive parcels of soil with others that strongly transmit but weakly retain water creates a net enhancing effect on the root-accessible soil's ability to retain water for an extended time, as is vital where infiltration is infrequent. In a desert, this sort of spatial heterogeneity may play a crucial role, allowing some portions of the soil to concentrate and retain water that might be unavailable to plants if the soil were less spatially variable.

Further hydrogeologic research on desert soils can provide needed advances in understanding and quantifying the relation between observable soil characteristics and their particular value to the quality of ecological habitat. For example, there is a need to evaluate conditions relative to the cooperative or competitive relationships among species as well as individuals. The fact that some alterations of particular hydraulic characteristics proceed monotonically with soil age, but others do not, means that the creation of property-transfer models based on soil age as an independent parameter will not be straightforward for all processes. A deeper understanding of the relation between fan-architectural and pedogenic features and physically and biologically important properties, such as the soil's ability to retain water against the processes of drainage and evaporation, will be a promising basis for practical means of estimating ecophysiological significant properties across large areas.

#### ACKNOWLEDGMENTS

We are grateful to the Mojave Desert DOI (Department of the Interior) on the Landscape Program for supporting this research. Debra Hughson of the National Park Service helped immensely with land-use permissions and execution of the field experiments. Kari Winfield, Sabrina Belknap, Sarah Robinson, Jane Duxbury, and Benjamin Mirus made important contributions to the planning and execution of the field experiments.

## References

- Andraski, B.J. 1997. Soil-water movement under natural-site and waste-site conditions: A multiple-year field study in the Mojave Desert, Nevada. *Water Resour. Res.* 33:1901–1916.
- Baumhardt, R.L., R.J. Lascano, and S.R. Evett. 2000. Soil material, temperature, and salinity effects on calibration of multisensor capacitance probes. *Soil Sci. Soc. Am. J.* 64:1940–1946.
- Bhark, E.W., and E.E. Small. 2003. Association between plant canopies and the spatial patterns of infiltration in shrubland and grassland of the Chihuahuan Desert, New Mexico. *Ecosystems* 6:185–196.
- Binley, A., G. Cassiani, R. Middleton, and P. Winship. 2002. Vadose zone flow model parameterisation using cross-borehole radar and resistivity imaging. *J. Hydrol.* 267:147–159.
- Breshears, D.D., and E.J. Barnes. 1999. Interrelationships between plant functional types and soil moisture heterogeneity for semiarid landscapes within the grassland/forest continuum: A unified conceptual model. *Landscape Ecol.* 14:465–478.
- Caldwell, T.G., E.V. McDonald, and M.H. Young. 2006. Soil disturbance and hydrologic response at the National Training Center, Ft. Irwin, California. *J. Arid Environ.* 67:456–472.
- Cassel, D.K., and D.R. Nielsen. 1986. Field capacity and available water capacity. p. 901–928. *In* A. Klute (ed.) *Methods of soil analysis*. Part 1. 2nd ed. SSSA Book Ser. 5. SSSA, Madison, WI.
- Caylor, K.K., and H.H. Shugart. 2006. Pattern and process in savanna ecosystems. p. 259–281. *In* P. D'Odorico and A. Porporato (ed.) *Dryland ecohydrology*. Springer, Dordrecht, the Netherlands.
- Constantz, J., and W.N. Herkelrath. 1984. Submersible pressure outflow cell for measurement of soil water retention and diffusivity from 5 to 950°C. *Soil Sci. Soc. Am. J.* 48:7–10.
- Daily, W., and E. Owen. 1991. Cross-borehole resistivity tomography. *Geophysics* 56:1228–1235.
- Day-Lewis, F.D., Y. Chen, and K. Singha. 2007. Moment inference from tomograms. *Geophys. Res. Lett.* 34: L22404, doi:10.1029/2007GL031621.
- Day-Lewis, F.D., S.K. Singha, and A. Binley. 2005. The application of petrophysical models to radar and electrical resistivity tomograms: Resolution-dependent limitations. *J. Geophys. Res.* 110:B08206, doi:10.1029/2004JB003569.
- DiCarlo, D.A. 2004. Experimental measurements of saturation overshoot on infiltration. *Water Resour. Res.* 40:W04215, doi:10.1029/2003WR002670.
- DiCarlo, D.A. 2006. Quantitative network model predictions of saturation behind infiltration fronts and comparison with experiments. *Water Resour. Res.* 42:W07408, doi:10.1029/2005WR004750.
- Gile, L.H., F.F. Peterson, and R.B. Grossman. 1966. Morphological and genetic sequences of carbonate formation in desert soils. *Soil Sci.* 101:347–360.
- Grayson, R.B., A.W. Western, F.H.S. Chiew, and G. Bloeschl. 1997. Preferred states in spatial soil moisture patterns: Local and nonlocal controls. *Water Resour. Res.* 33:2897–2908.
- Grayson, R.B., A.W. Western, J.P. Walker, D.D. Kandel, J.F. Costelloe, and D.J. Wilson. 2006. Controls on patterns of soil moisture in arid and semi-arid systems. p. 109–127. *In* P. D'Odorico and A. Porporato (ed.) *Dryland ecohydrology*. Springer, Dordrecht, the Netherlands.
- Hamerlynck, E.P., J.R. McAuliffe, E.V. McDonald, and S.D. Smith. 2002. Ecological responses of two Mojave Desert shrubs to soil horizon development and soil water dynamics. *Ecology* 83:768–779.
- Hillel, D. 1998. *Environmental soil physics*. Academic Press, San Diego.
- Katul, G.G., A. Porporato, E. Daly, A.C. Oishi, H.-S. Kim, P.C. Stoy, J.-Y. Juang, and M.B. Siqueira. 2007. On the spectrum of soil moisture from hourly to interannual scales. *Water Resour. Res.* 43(5):W05428, doi:10.1029/2006WR005356.
- LaBrecque, D.J., M. Miletto, W. Daily, A. Ramirez, and E. Owen. 1996. The effects of noise on Occam's inversion of resistivity tomography data. *Geophysics* 61:538–548.
- Lohse, K.A., and W.E. Dietrich. 2005. Contrasting effects of soil development on hydrological properties and flow paths. *Water Resour. Res.* 41(12):W12419, doi:10.1029/2004WR003403.
- Lombardini, L. 2006. Ecophysiology of plants in dry environments. p. 47–65. *In* P. D'Odorico and A. Porporato (ed.) *Dryland ecohydrology*. Springer, Dordrecht, the Netherlands.
- McDonald, E.V., F.B. Pierson, G.N. Flerchinger, and L.D. McFadden. 1996. Application of a soil-water balance model to evaluate the influence of Holocene climate change on calcic soils, Mojave Desert, California, U.S.A. *Geoderma* 74:167–192.
- Meadows, D.G., M.H. Young, and E.V. McDonald. 2008. Influence of relative surface age on hydraulic properties and infiltration on soils associated with desert pavements. *Catena* 72:169–178.
- Miller, D.M., D.R. Bedford, D.L. Hughson, E.V. McDonald, S.E. Robinson, and K.M. Schmidt. 2009. Mapping Mojave Desert ecosystem properties with surficial geology. p. 225–251. *In* R.H. Webb et al (ed.) *The Mojave Desert: Ecosystem processes and sustainability*. Univ. of Nevada Press, Reno.
- Mirus, B.B., K.S. Perkins, J.R. Nimmo, and K. Singha. 2009. Hydrologic characterization of desert soils with varying degrees of pedogenesis: 2. Inverse modeling for unsaturated hydraulic properties. *Vadose Zone J.* 8:497–510 (this issue).
- Moysey, S., K. Singha, and R. Knight. 2005. Inferring field-scale rock physics relations through numerical simulation. *Geophys. Res. Lett.* 32:L08304, doi:10.1029/2004GL022152.
- Nimmo, J.R., and K.S. Perkins. 2008. Effect of soil disturbance on recharging fluxes: Case study on the Snake River Plain, Idaho National Laboratory, USA. *Hydrogeol. J.* 16:829–844, doi:10.1007/s10040-007-0261-2.
- Nimmo, J.R., K.M. Schmidt, K.S. Perkins, and J.D. Stock. 2009. Rapid measurement of field-saturated hydraulic conductivity for areal characterization. *Vadose Zone J.* 8:142–149.

- Odening, W.R., B.R. Strain, and W.C. Oechel. 1974. The effect of decreasing water potential on net CO<sub>2</sub> exchange of intact desert shrubs. *Ecology* 55:1086–1095.
- Ogle, K., and J. Reynolds. 2004. Plant responses to precipitation in desert ecosystems: Integrating functional types, pulses, thresholds, and delays. *Oecologia* 141:282–294.
- Scanlon, B.R., K. Keese, R.C. Reedy, J. Simunek, and B.J. Andraski. 2003. Variations in flow and transport in thick desert vadose zones in response to paleoclimatic forcing (090 kyr): Field measurements, modeling, and uncertainties. *Water Resour. Res.* 39(7):1179, doi:10.1029/2002WR001604.
- Schulze, E.D., E. Beck, and K. Müller-Hohenstein. 2005. *Plant ecology*. Springer-Verlag, Berlin.
- Shafer, D.S., M.H. Young, S.F. Zitzer, T.G. Caldwell, and E.V. McDonald. 2007. Impacts of interrelated biotic and abiotic processes during the past 125 000 years of landscape evolution in the northern Mojave Desert, Nevada, USA. *J. Arid Environ.* 69:633–657.
- Shiozawa, S., and H. Fujimaki. 2004. Unexpected water content profiles under flux-limited one-dimensional downward infiltration in initially dry granular media. *Water Resour. Res.* 40:W07404, doi:10.1029/2003WR002197.
- Singha, K., F.D. Day-Lewis, and S. Moysey. 2007. Accounting for tomographic resolution in hydrogeophysical data. p. 227–242. *In* D.W. Hyndman et al. (ed.) *Subsurface hydrology: Data integration for properties and processes*. Geophys. Monogr. Ser. 171. Am. Geophys. Union, Washington, DC.
- Singha, K., and S.M. Gorelick. 2005. Saline tracer visualized with electrical resistivity tomography: Field scale moment analysis. *Water Resour. Res.* 41:W05023, doi:10.1029/2004WR003460.
- Slater, L., A.M. Binley, W. Daily, and R. Johnson. 2000. Cross-hole electrical imaging of a controlled saline tracer injection. *J. Appl. Geophys.* 44:85–102.
- SSSA. 1997. *Glossary of soil science terms 1996*. SSSA, Madison, WI.
- Sternberg, P.D., M.A. Anderson, R.C. Graham, J.L. Beyers, and K.R. Tice. 1996. Root distribution and seasonal water status in weathered granitic bedrock under chaparral. *Geoderma* 72:89–98.
- Stonestrom, D.A., and K.C. Akstin. 1994. Nonmonotonic matric pressure histories during constant flux infiltration into homogeneous profiles. *Water Resour. Res.* 30:81–91.
- Tripp, A.C., G.W. Hohmann, and C.M. Swift, Jr. 1984. Two-dimensional resistivity inversion. *Geophysics* 49:1708–1717.
- Ursino, N. 2007. Modeling banded vegetation patterns in semiarid regions: Interdependence between biomass growth rate and relevant hydrological processes. *Water Resour. Res.* 43:W04412, doi:10.1029/2006WR005292.
- Young, M.H., E.V. McDonald, T.G. Caldwell, S.G. Benner, and D.G. Meadows. 2004. Hydraulic properties of a desert soil chronosequence in the Mojave Desert, USA. *Vadose Zone J.* 3:956–963.
- Youngs, E.G. 1987. Estimating hydraulic conductivity values from ring infiltrometer measurements. *J. Soil Sci.* 38:623–632.